Strong room-temperature ferromagnetism of high-quality lightly Mn-doped ZnO grown by molecular beam epitaxy

Zheng Zuo,[1] Huimei Zhou,[1] Mario J. Olmedo,[1] Jieying Kong,[1] Ward P. Beyermann,[2] Jian-Guo Zheng,[3] Yan Xin,[4] and Jianlin Liu[1,a)]
[1]*Quantum Structures Laboratory, Department of Electrical Engineering, University of California - Riverside, Riverside, California 92521, USA*
[2]*Department of Physics and Astronomy, University of California - Riverside, Riverside, California 92521, USA*
[3]*Laboratory for Electron and X-ray Instrumentation, California Institute for Telecommunications and Information Technology, University of California - Irvine, Irvine, California 92697, USA*
[4]*NHMFL, Florida State University, 1800 E. Paul Dirac Dr., Tallahassee, Florida 32310-3706, USA*

(Received 26 March 2012; accepted 17 July 2012; published online 5 September 2012)

Strong room-temperature ferromagnetism is demonstrated in single crystalline Mn-doped ZnO grown by molecular beam epitaxy. With a low Mn concentration of 2×10^{19} cm^{-3}, Mn-doped ZnO films exhibited room-temperature ferromagnetism with a coercivity field larger than 200 Oe, a large saturation moment of 6 μ_B/ion, and a large residue moment that is ~70% of the saturation magnetization. Isolated ions with long range carrier mediated spin-spin coupling may be responsible for the intrinsic ferromagnetism. © *2012 American Institute of Physics*.
[http://dx.doi.org/10.1063/1.4749397]

INTRODUCTION

Diluted magnetic semiconductor (DMS) has been proposed for more than two decades and has attracted much attention for its potential in spintronic applications,[1] such as logic process, memory storage, communication, and quantum computation.[2–4] ZnO and GaN have been predicted to be candidates of room-temperature DMS,[1,3–5] and extensive work has been performed on transition metal (TM) doped ZnO synthesized using various methods, including chemical reaction,[6,7] sintering,[8,9] ion implantation,[10–12] sputtering,[13] pulsed laser deposition,[14] metal-organic chemical vapor deposition,[15] and molecular beam epitaxy (MBE).[16,17] One major problem concerning TM doped ZnO is whether the ferromagnetism is associated with clusters of the TM dopant. Although Mn-doped ZnO lacks room-temperature ferromagnetic Mn-rich phases,[19] almost all kinds of behaviors have been reported by different groups, such as being non-magnetic,[7] paramagnetic,[13] ferromagnetic,[8] antiferromagnetic,[18] and spin-glass like.[14] In addition, the mechanism responsible for these states is controversial. There have been various models trying to explain magnetic semiconductor systems, including p-d exchange Zener model,[20] bound magnetic polaron,[21,22] F centers,[23] etc. While there have been various experimental reports supporting one model or another,[6–18] reproducibility between different groups remains in question, indicating very high sensitivity of magnetic properties on the growth conditions. Here we report MBE growth of high-quality single crystalline Mn-doped ZnO with very low Mn concentration and their magnetic properties. Strong above room-temperature intrinsic ferromagnetism is demonstrated. The results may be explained by singular ion induced intrinsic ferromagnetism mechanism.

a)Author to whom correspondence should be addressed. Electronic mail: jianlin@ee.ucr.edu. Tel.: +1-951-8277131. Fax: +1-951-8272425.

EXPERIMENTS

The Mn-doped ZnO thin films were grown using electron cyclotron resonance (ECR)-MBE. Radical Knudsen effusion cells filled with elemental Zn (6N) and Mn (5.5N) metals were used as Zn and Mn sources. The Zn and Mn fluxes were controlled by the effusion cell temperatures. An ECR plasma tube supplied with O_2 (5N) gas was used as the oxygen source, and the oxygen flow rate was precisely tuned by a mass flow controller. The films were grown on r-sapphire substrates (Rubicon). The substrates were cleaned in boiling aqua regia solution for 50 min before DI water rinsing and blown dry by nitrogen. Samples were then annealed in vacuum at 800 °C for 30 min. A low temperature ZnO buffer was grown at 450 °C. The buffer growth lasted 5 min with an estimated thickness of 1–2 nm. During the growth, the Zn cell temperature and O_2 flow rate were kept at 430 °C and 14 sccm, respectively. For Mn doped samples the Mn cell temperature was set at 750 °C. The substrate temperature was 650 °C, and the growths lasted 2 h. An annealing at 800 °C for 30 min was performed after growth in vacuum. A reference sample was grown with the same growth procedure without Mn flux. The thickness of the films was measured using a Dektak 8 Surface Profilometer. X-ray diffraction (XRD) measurements were performed using a Bruker D8 Advance x-ray diffractometer. The photoluminescence (PL) study was carried out using a home-built PL system with a Janis cryostat, with a 325-nm He-Cd laser for the excitation source and a photomultiplier tube for the PL detection. Energy dispersive x-ray (EDX) and scanning electron microscopy (SEM) were done using an Oxford/INCA SEM system. Atomic force microscopy (AFM) and magnetic force microscopy (MFM) measurement were done with a Veeco/Bruker AFM with a Co coated MFM tip in tapping mode. Cross-sectional TEM specimens were prepared in a FEI Quanta 3D FEG dual-beam FIB and diffraction

contrast TEM imaging, and selected area electron diffraction (SAED) were carried out in a FEI/Philips CM-20 TEM at the materials characterization facility (LEXI) in UC Irvine. High-resolution TEM and Z-contrast STEM work was performed in a JEOL JEM ARM200F TEM at the Florida State University. The magnetic properties of the samples were characterized using a quantum design MPMS SQUID magnetometer with the magnetic field parallel to the film plane. Samples were cut into rectangles with dimensions of 6 mm $\times$ 8 mm and mounted in a non-magnetic straw during the measurement.

RESULTS AND DISCUSSION

Both un-doped and doped ZnO samples have similar thicknesses of $\sim$35 nm, measured with a profilometer. This number was also confirmed by secondary ion mass spectrometry (SIMS) and TEM results. Figures 1(a) and 1(b) show reflective high energy electron diffraction (RHEED) patterns acquired in the MBE system at room temperature after the growth. The un-doped sample shows a streaky pattern indicating a smooth surface, while Mn-doped sample shows slightly widened streaks, indicating deviation from flat surface. SEM images were acquired for both samples,[24] and the surfaces are smooth and featureless. The AFM image of a Mn-doped ZnO sample (Figure 1(c)) shows long stripes with $\sim$0.5 μm spacing, which is similar to the pattern of single crystal ZnO surface after thermal treatment, as reported by Meyer *et al.*[25] Similar stripe pattern has been reported on annealed sapphire substrate,[26] so there is a possibility that these patterns may be inherited from the atomic steps on the wafer surface as a result of thermal treatment, considering that the ZnO film is very thin. The roughness (rms) is 0.7 nm within a 10 μm $\times$ 10 μm scan range. Figure 1(d) shows a phase image of a MFM measurement, obtained with a lift distance of 80 nm during the AFM measurement. The image shows no evident signal of perpendicular magnetic moment. Since Mn-rich clusters would tend to randomly align, lack of perpendicular moment indicates no evident clustering.

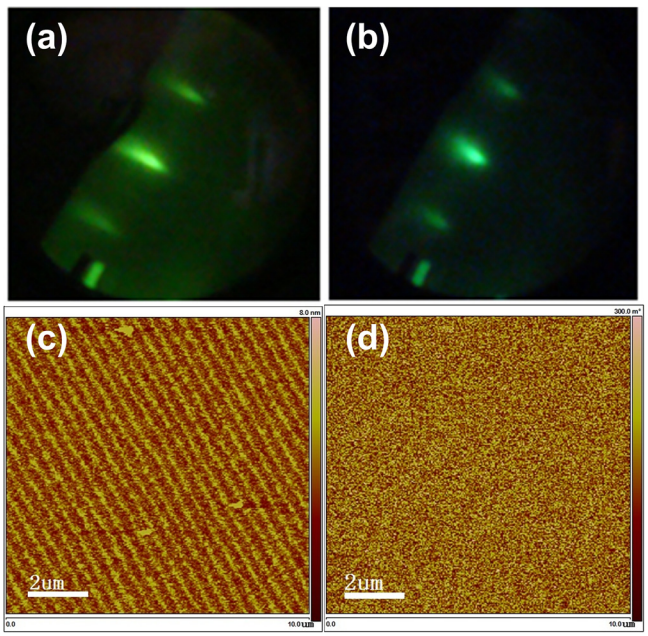

FIG. 1. Streaky RHEED patterns at 4 kV of (a) un-doped ZnO, and (b) Mn doped ZnO showing smooth surface for both samples. (c) AFM image of Mn doped ZnO showing stripe-like surface pattern, (d) MFM image of Mn doped ZnO showing no evident perpendicular moment.

To further confirm that there are no Mn-rich clusters in the Mn-doped sample, cross-sectional TEM experiments were carried out. Figures 2(a) and 2(b) show bright-field and weak-beam images of the Mn-doped ZnO film grown on sapphire substrate. These images display line defects (dislocations) in the film, but no Mn-rich clusters were observed. Figure 2(c) is a typical SAED pattern from both the film and substrate, where the substrate was tilted to its zone axis and the film was slightly away from its zone axis. There are only two sets of the diffract spots present, highlighted by solid lines and by dash lines, corresponding to the substrate and the film, respectively. The pattern indicates that the film is single crystal and the $(11\bar{2}0)$ plane of the film is parallel to the $(1\bar{1}02)$ plane of the substrate, which fits the epitaxial relationship of ZnO grown on r-sapphire.[27] Figure 2(c) also indicates that there are no other phases including Mn-rich clusters in the film. Figures 2(d) and 2(e) are typical high-resolution TEM and Z-contrast STEM images, respectively, with the ZnO film tilted exactly along its zone axis, and the substrate is 4.4° off its zone axis. The individual brighter dots in the Z-contrast STEM image (Fig. 2(e)) are the Zn atomic columns of the film, and the lower intensity lines are the Al atomic columns of the substrate. It shows that the single crystalline ZnO film has an epitaxy growth on the substrate. The film/substrate interface is flat and abrupt at atomic scale.

Figures 3(a) and 3(b) show XRD spectra of Mn-doped ZnO and un-doped ZnO, respectively. The θ-2θ scan shows peaks for r-sapphire $(1\bar{1}02)$ as well as A-plane $(11\bar{2}0)$ ZnO. None of the other ZnO directions are observed due to the high-quality epitaxial growth by MBE. No peak shift is observed between the doped and un-doped ZnO samples. No Mn-rich secondary phases are detected within detection limit.

Various methods were implemented to assess the Mn concentration of the thin film. Both EDX and XPS results showed no trace of Mn,[24] which would appear if there was a significant amount of clustered Mn. STEM with nanometer electron probe was also used to detect elements from different areas of the film, and no Mn signal was detected, indicating that the Mn signal was below the detection limit and no Mn-related clusters were developed in the film. Figure 4 shows SIMS spectrum, in which a $\sim 2 \times 10^{19}$ cm^{-3} Mn concentration is acquired. This leads to a number of $\sim$0.04% at Mn content.

Figures 5(a) and 5(b) show temperature-dependent PL spectra of un-doped and Mn-doped ZnO. At 15 K both samples show a dominant peak at $\sim$3.362 eV with a broad mixture of luminescence in the 3.3-3.2 eV region. As the temperature increases, the high energy peak blue-shifts to $\sim$3.384 eV, evident at around 60 K. Further increase of temperature induces a typical red shift due to temperature-induced band-gap shrinkage. Figure 6(a) shows polarization-dependent PL spectra of the Mn-doped ZnO.[24] Coexistence of two peaks (3.362 eV and 3.384 eV) at 15 K and a clear polarization dependence of

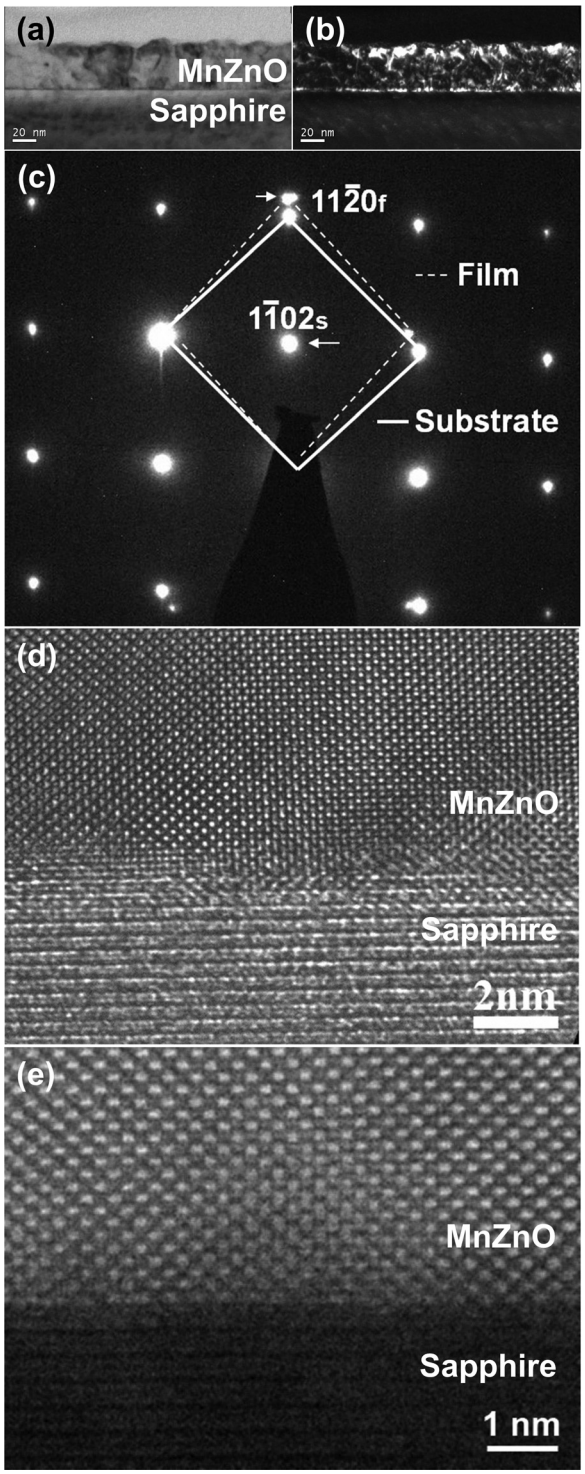

FIG. 2. TEM images under (a) bright field and (b) weak beam conditions of Mn doped ZnO, showing no Mn clusters and other secondary phases but line defects. c) SAED pattern of Mn doped ZnO sample, showing patterns from both sapphire and ZnO. The pattern explains the expected epitaxial relationship and single crystal growth. (d) High-resolution TEM image and (e) Z-contrast STEM image of Mn doped ZnO sample cross section. Z-contrast image shows that the interface between sapphire and ZnO is atomic level flat.

the two peaks are evident, as predicted for a perpendicular incident beam against the c-axis.[28] The two peaks show up at different excitation polarization that is ~90° apart, while the general behavior evolves at a period of 180°. This behavior

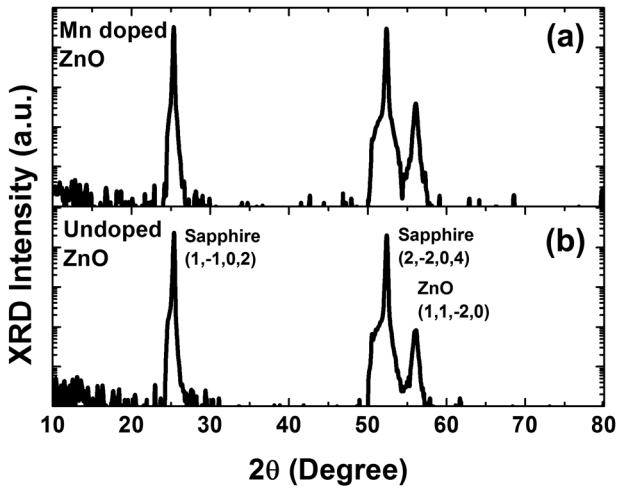

FIG. 3. XRD spectra of (a) Mn doped ZnO and (b) un-doped ZnO. Besides substrate related peaks, only ZnO $(11\bar{2}0)$peak was observed, indicating that the ZnO growth direction is parallel to the normal of the $(11\bar{2}0)$ plane. No evident peak shift or Mn-rich secondary phases are present in Mn doped ZnO.

fits the symmetry model as predicted by Reynalds *et al.*[29] Figure 6(b) is intensity plot of the polarization dependent PL data. The high energy edge shift is evident, while the broad luminescence around 3.25 eV shifts along with the high energy edge, indicating related origin. The observation of this fine structure split upon different polarization confirms an A-plane epitaxial growth of single crystalline ZnO wurtzite structure. For the exciton related peaks there are no qualitative difference between the doped and un-doped samples, supporting the very low doping concentration claim and the doped film remains close to its intrinsic semiconductor nature. It is reasonable to believe that the 3.362 eV and 3.384 eV peaks are of the same donor bound origin. Assume the sample is still following the polarization selection rule under unstrained situation, 3.362 eV can be assigned to A/B band donor bound exciton and 3.384 eV to C band. This means ~22 meV energy difference between A/B and C band, which is much different from reported value ~45 meV.[27] Under normal unstrained circumstances, the energy split between A/B band and C band is

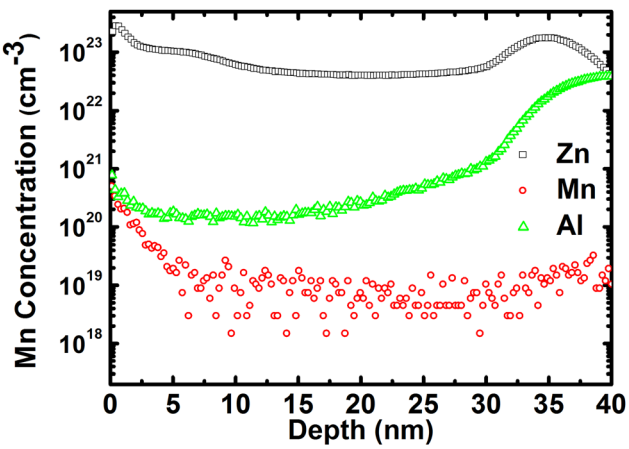

FIG. 4. SIMS spectrum of Mn doped ZnO sample giving Mn concentration of ~0.04 at. %. Mn concentration is aligned through Zn signal. The numbers for Zn and Al are arbitrary.

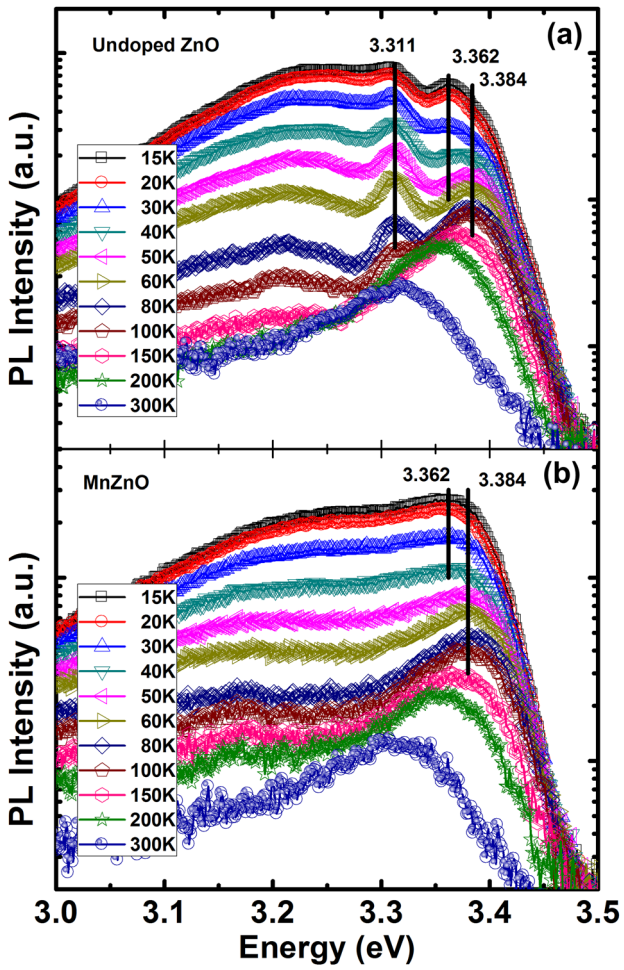

FIG. 5. Temperature dependent photoluminescence of (a) un-doped ZnO and (b) Mn doped ZnO. The persistent 3.384 eV peak is assigned to C band bound exciton.

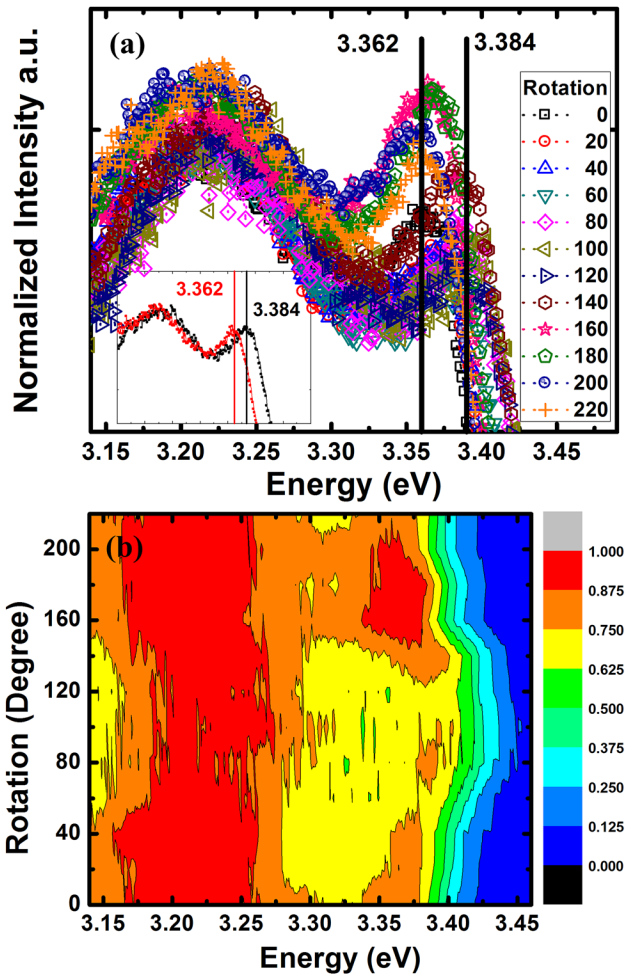

FIG. 6. (a) Polarization dependent PL of Mn-doped ZnO sample measured at 15 K. The rotation in degrees denotes the position of a Glan-Tyler type polarizer, thus the polarization of excitation source. Insert is PL at polarizer rotation of 140 and 220, respectively, to clearly show the difference of peak energy. (b) Intensity plot of polarization dependent PL data in (a). The peak shift at high energy edge is evident while the luminescence bump at ~3.25 eV shifts together with the higher energy peak, indicating related origin. Note that PL intensity has been normalized.

attributed to crystal field while the energy split between A and B band is due to spin-orbit coupling. It is predicted that under anisotropic strain in c-plane, the exciton bands will bend, deform, and cross-over, especially evident with the A and B bands.[29,30] Thus the larger energy change may indicate a larger spin-orbit term, which will affect magnetic property of the thin film. The exact assignment of the observed peaks requires further examination and analysis.

The magnetic moment as a function of the applied magnetic field was acquired at different temperatures for both doped and un-doped samples. Figure 7(a) shows the measurement for the un-doped ZnO sample. No ferromagnetic behavior was observed within the measurement temperature range (10 K-300 K). The data shows diamagnetic behavior, which can come from several sources. No "unintentionally doped" ZnO ferromagnetism was observed, and our sample preparation process before measurement did not result in ferromagnetism. The Mn doped sample shows ferromagnetic behavior over the entire temperature range. Figure 7(b) shows M-H hysteresis loop after removal of a linear response term. The measured moment was normalized to per unit ion (i.e., μ_B/ion) utilizing the Mn concentration determined from the SIMS data. At room temperature, the saturation moment (M_s) is ~6 μ_B/ion, while the coercivity field is larger than 200 Oe. The saturation moment does not vary much as the temperature is reduced, while the coercivity field does increase at lower temperatures. At 10 K the coercivity field is larger than 500 Oe. It should be noted that the sample has a much higher remnant moment at zero field (M_r). The M_r/M_s ratio reaches ~70% at 300 K, much larger than our previously reported MnZnO samples,[8] which makes the M-H loop more of a square shape like those of hard magnets. Hard hysteresis loops are rarely observed in Mn doped ZnO, and this is desirable for applications involving the storage of information. We also performed temperature scans on the Mn doped ZnO sample. Due to the diamagnetic background, field cooling (FC) measurements were performed at two fields: 1000 Oe and 2000 Oe. Both measurements were done with a history field of 6000 Oe. Zero field cooling (ZFC) measurement was also carried out with the same history field of 6000 Oe. As shown in Figure 7(c), there are no sharp maximum in the data for all three measurements between 20 K and 300 K, eliminating the possibility of several Mn-rich phases with Curie/Neel temperatures in the range from 40 K

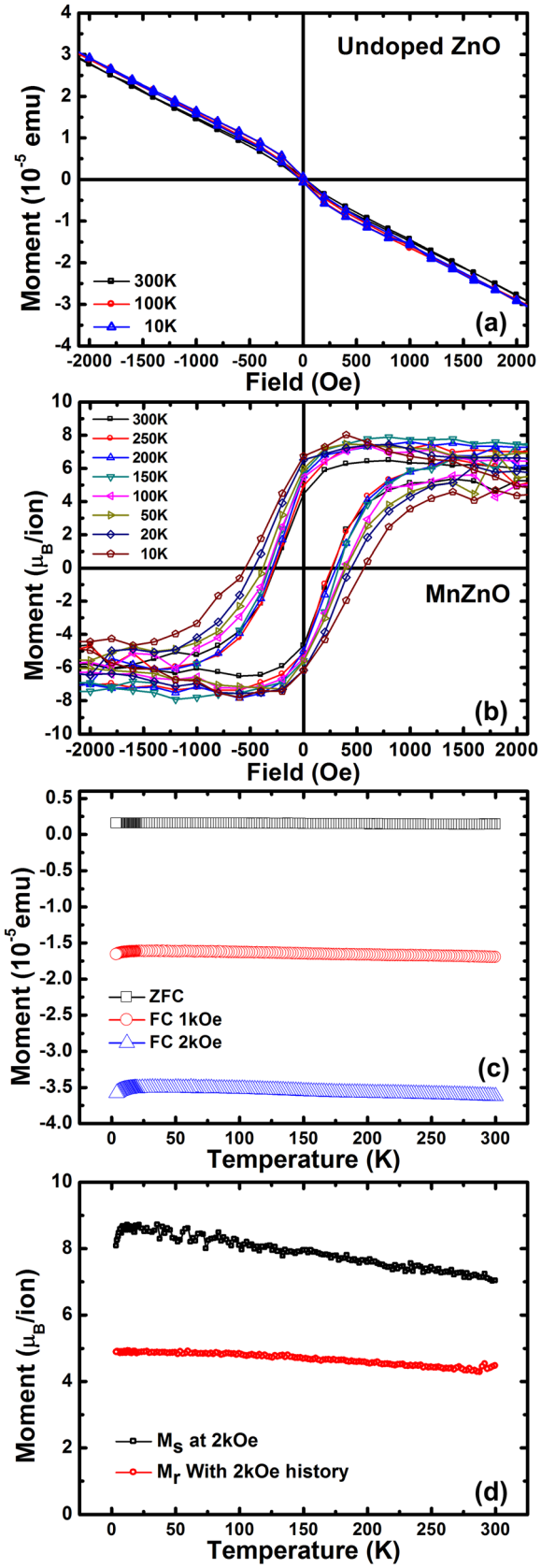

FIG. 7. (a) M-H graph of un-doped ZnO showing diamagnetic behavior with no ferromagnetism. (b) Hysteresis loop of Mn doped ZnO after subtraction of linear term, showing strong room temperature ferromagnetism, (c) ZFC and FC measurement results of Mn doped ZnO showing no abrupt phase change down to 10 K, (d) extracted saturation moment M_s and remnant moment at zero field M_r, indicating persistent ferromagnetism with high Currie temperature.

to 120 K.[18] There seems to be a phase transition at around 20 K, the origin of which remains to be clarified as no specific Mn-rich phase showing transition was reported at this temperature. Assuming a strictly linear term for the diamagnetism, M_s, the saturation moment at 2000 Oe can be assessed. Figure 7(d) shows M_s and M_r plotted against temperature. M_r is obtained directly from ZFC data. The data matches reasonably well with that from hysteresis loop measurements shown in Figure 7(b). From the trend shown in Figure 7(d), Mn doped ZnO has a very large Currie temperature making it applicable for room temperature devices.

Large remnant moment ratio is attributed to the single crystalline nature of the film. According to classical magnetism, for a given measurement, the measured coercivity field and remnant moment will depend on the geometric alignment of the external field against the easy axis of the object, as well as internal "'pinning" of domain walls. The remnant moment is maximized when the external field is aligned with internal easy axis thus making rotation and flipping of magnetic moment most difficult. For a polycrystalline thin film, the easy axis of each crystal domain will be random; some portion of the domains would always be misaligned against a given external field. Thus the M_r/M_s ratio of such systems would tend to be lower. Through the advantage of single-crystal thin film growth by MBE, the easy axis of the thin film is aligned along a single direction; therefore ratios of M_r/M_s as high as ~70% are achieved. The saturation moment of ~6 μ_B/ion at room temperature is larger but quite close to the results acquired with the ion-implantation method we reported before.[11] Our assumption is that Mn would substitute Zn site in the crystal and thus have valence of 2+. Mn^{2+} ion configuration is $3d^5$, thus five unpaired electrons are at the 3d orbit. Based on the classical calculation $|m| = g'J\mu_B$, $g' = 1 + \frac{J(J+1)+s(s+1)-L(L+1)}{2J(J+1)}$, for $3d^5$, the maximum moment is 5 uB. So we believe our results are marginally correct for a scenario of isolated Mn ion assuming that real Mn concentration may be slightly higher than the SIMS data. With a Mn concentration of 2×10^{19} cm^{-3}, the average ion to ion distance would be ~3 nm, which is too large to allow super-exchange or double exchange to take place. Treating Mn ions as singular isolated ion would be more feasible, thus explaining the large μ_B/ion value. It is worth noting that an earlier report by Kittilstved *et al.* on a Mn doped ZnO with a 0.2% concentration did report a μ_B/ion value larger than 1.[31] The Mn dopant concentration in the present sample is very low; therefore, bound magnetic polaron model might have difficulty to apply, since it practically depends on double-exchange and there are no other dopants available to act as intermediate moment host. As recently addressed by Dietl,[20] carrier mediated indirect coupling is possible based on a modified p-d Zener model to provide room temperature ferromagnetism. Such a mechanism allows larger ion-ion distances, although the actual limit of such an assumption remains unexplored. Nevertheless, considering the fact that semiconductor can have orders of magnitude large spin coherence time than metals,[2] a long distance indirect coupling is not totally unwarranted.

Finally we briefly comment on the doping concentration effect on magnetic properties. Low-Mn-concentration ferromagnetism was rarely studied while high-Mn-concentration ferromagnetism is commonly reported in literature. Heavily Mn-doped ZnO thin films usually contain clustering and phase segregation due to low solubility of Mn in ZnO. It is possible that the measured ferromagnetism was offset partially by non-magnetic or paramagnetic Mn phases. The existence of such Mn phases could be substantial enough to reduce the μ_B/ion value. Also, with larger Mn concentration, the Mn-ions are close enough to enable super-exchange or double exchange coupling, which would provide a smaller μ_B/ion number.[20] Thus the reported behaviors can be reconciled, and optimized Mn doping condition toward perfect ferromagnetic properties may be acquired at lower Mn concentration, instead of higher ones.

CONCLUSION

We have observed strong room temperature ferromagnetism with very low doping concentration of Mn ion in ZnO thin films. The Mn concentration is well below the reported solubility limit and minimizes the chances for secondary phase formation. The magnetic behavior is found to have a fairly large coercivity field of 200 Oe as well as very large remnant moment of 70%. The normalized moment of 6 μ_B/ion is so large that only an isolated moment explanation is reasonable, which also matches the large mean distance between ions inferred from the low Mn concentration. The result supports intrinsic ferromagnetism of Mn doped ZnO induced by singular Mn ions.

ACKNOWLEDGMENTS

This material is based on research sponsored by DARPA/Defense Microelectronics Activity (DMEA) under Agreement No. H94003-10-2-1004. The TEM facility at FSU is funded and supported by the Florida State University Research Foundation, National High Magnetic Field Laboratory (NSF-DMR-0654118) and the State of Florida.

[1]T. Dietl, H. Ohno, F. Matsukura, J. Cibert, and D. Ferrand, Science **287**, 1019 (2000).
[2]D. D. Awschalom and M. E. Flatte, Nat. Phys. **3**, 153 (2007).
[3]S. B. Ogale, Adv. Mater. **22**, 3125 (2010).
[4]Y. F. Tian, S. R. Bakaul, and T. Wu, Nanoscale **4** 1529 (2012).
[5]K. Sato and H. Katayama-Yoshida, Jpn. J. Appl. Phys. **40**, L334 (2001).
[6]S. W. Jung, S. J. An, G.-C. Yi, C. U. Jung, S.-I. Lee, and S. Cho, Appl. Phys. Lett. **80**, 4561 (2002).
[7]J. Alaria, P. Turek, M. Bernard, M. Bouloudenine, A. Berbadj, N. Brihi, G. Schmerber, S. Colis, and A. Dinia, Chem. Phys. Lett. **415**, 337 (2005).
[8]P. Shama, A. Gupta, K. V. Rao, F. J. Owens, R. Shama, R. Ahuja, J. M. O. Guillen, B. Johansson, and G. A. Gehring, Nat. Mater. **2**, 673 (2003).
[9]Y. F. Tian, Y. F. Li, M. He, I. A. Putra, H. Y. Peng, B. Yao, S. A. Cheong, and T. Wu, Appl. Phys. Lett. **98**, 162503 (2011).
[10]D. P. Norton, M. E. Overberg, S. J. Pearton, K. Pruessner, J. D. Budai, L. A. Boatner, M. F. Chisholm, J. S. Lee, Z. G. Khim, Y. D. Park, and R. G. Wilson, Appl. Phys. Lett. **83**, 5488 (2003).
[11]Z. Yang, J. L. Liu, M. Biasini, and W. P. Beyermann, Appl. Phys. Lett. **92**, 042111 (2008).
[12]Z. Yang, W. P. Beyermann, M. B. Katz, O. K. Ezekoye, Z. Zuo, Y. Pu, J. Shi, X. Q. Pan, and J. L. Liu, J. Appl. Phys. **105**, 053708 (2009).
[13]X. M. Cheng and C. L. Chien, J. Appl. Phys. **93**, 7876 (2003).
[14]T. Fukumura, Z. Jin, M. Kawasaki, T. Shono, T. Hasegawa, S. Koshihara, and H. Koinuma, Appl. Phys. Lett. **78**, 958 (2001).
[15]C. Tuan, J. D. Bryan, A. B. Pakhomov, V. Shutthanandan, S. Thevuthasan, D. E. Mccready, D. Gaspar, M. H. Engelhard, J. W. Rogers, Jr., K. Krishnan, D. R. Gamelin, and S. A. Chambers, Phys. Rev. B **70**, 054424 (2004).
[16]X. J. Wang, I. A. Buyanova, W. M. Chen, C. J. Pan, and C. W. Tu, J. Appl. Phys. **103**, 023712 (2008).
[17]Z.Yang, Z. Zuo, H. Zhou, W. P. Beyermann, and J. Liu, J. Cryst. Growth **314**, 97 (2011).
[18]G. Lawes, A. S. Risbud, A. P. Ramirez, and R. Seshadri, Phys. Rev. B **71**, 045201 (2005).
[19]C. Liu, F. Yun, and H. Morkoc, J. Mater. Sci.: Mater. Electron. **16**, 555 (2005).
[20]T. Dietl, Nat. Mater. **9**, 965 (2010).
[21]J. M. D. Coey, M. Venkatesan, and C. B. Fitzgerald, Nat. Mater. **4**, 173 (2005).
[22]A. C. Durst, R. N. Bhatt, and P. A. Wolff, Phys. Rev. B **65**, 235205 (2002).
[23]Q. Wang, Q. Sun, P. Jena, and Y. Kawazoe, Phys. Rev. B **79**, 115407 (2009).
[24]See supplementary material at http://dx.doi.org/10.1063/1.4749397 for additional experimental results and experiment configuration.
[25]S. Graubner, C. Neumann, N. Volbers, B. K. Meyer, J. Bläsing, and A. Krost, Appl. Phys. Lett. **90**, 042103 (2007).
[26]H. Komurasaki, T. Isono, T. Tsukamoto, and T. Ogino, Appl. Surf. Sci. **258**, 5666 (2012).
[27]Ü. Özgür, Ya. I. Alivov, C. Liu, A. Teke, M. A. Reshchikov, S. Doğan, V. Avrutin, S.-J. Cho, and H. Morkoç, J. Appl. Phys. **98**, 041301 (2005).
[28]A. Teke, Ü. Özgür, S. Doğan, X. Gu, H. Morkoç, B. Nemeth, J. Nause, and H. O. Everitt, Phys. Rev. B **70**, 195207 (2004).
[29]D. C. Reynolds, D. C. Look, B. Jogai, C. W. Litton, G. Cantwell, and W. C. Harsch, Phys. Rev. B **60**, 2340 (1999).
[30]S. Ghosh, P. Waltereit, O. Brandt, H. T. Grahn, and K. H. Ploog, Phys. Rev. B **65**, 075202 (2002).
[31]K. R. Kittilstved, N. S. Norberg, and D. R. Gamelin, Phys. Rev. Lett. **94**, 147209 (2005).